Bulletin of Earthquake Engineering (2020) 18:821–836
https://doi.org/10.1007/s10518-018-00533-9

ORIGINAL RESEARCH

Ground motion amplification atop the complex sedimentary basin of Haifa Bay (Israel)

Shahar Shani-Kadmiel[1,4] · Omri Volk[1,5] · Zohar Gvirtzman[2] · Michael Tsesarsky[3]

Received: 2 September 2018 / Accepted: 29 November 2018 / Published online: 6 December 2018

Abstract
The Zevulun Valley (ZV) is a sedimentary basin underlying the heavily populated and industrialized petrochemical hub of Haifa Bay, Israel. With active tectonic faults at close range and a mixture of large population and vulnerable facilities, the seismic risk in the ZV is high. However, until now the national seismic network in Israel only included rock stations with no measurements supporting the expected difference between the ZV and its surroundings. Moreover, a detailed analysis of ground motions atop sedimentary basins using earthquakes data was never conducted in Israel for any basin. In this paper, we present a dataset collected during a 16 months monitoring campaign with a transportable network deployed in the ZV. For the first time in Israel we simultaneously recorded earthquake ($3.1 < Mw < 5.5$) ground motions at basin- and reference-sites. Spectral ratios reveal amplification factors tangibly higher than those previously reported by horizontal-to-vertical-spectral-ratio (HVSR) techniques and 2-D modeling. In particular, the deeper parts of the valley exhibit ground motion amplification up to a factor of 8 at frequencies lower than 1 Hz. Comparison of the measured spectral ratios with the results of 1-D linear-elastic analysis shows partial correlation reflecting the complexity of the sub-surface structure.

Keywords Ground motion · Amplification · Spectral ratio · Sedimentary basin · Haifa Bay

✉ Michael Tsesarsky
michatse@bgu.ac.il

[1] Department of Geological and Environmental Sciences, Ben-Gurion University of the Negev, Beersheba, Israel

[2] Geological Survey of Israel, Jerusalem, Israel

[3] Department of Structural Engineering, Ben-Gurion University of the Negev, Beersheba, Israel

[4] Present Address: Department of Geoscience and Engineering, Faculty of Civil Engineering and Geosciences, Delft University of Technology, Delft, The Netherlands

[5] Present Address: Department of Earth Sciences, Cambridge University, Cambridge, UK

1 Introduction

Measurements and damage observations of large earthquakes atop sedimentary basins have shown locally intensified ground motion (Gutenberg 1957; Aki and Larner 1970; Borcherdt 1970; Hudson 1972; Trifunac and Udwadia 1974; Gao et al. 1996; Alex and Olsen 1998; Graves et al. 1998; Hartzell et al. 2010). In Mexico City, Los Angeles and Kobe, megacities situated over large sedimentary basins, violent ground motions and prolonged shaking duration caused considerable structural damage and loss of life.

Various methods for local basin-site response estimation have been introduced over time; Instrumental methods, rooted in measurement of seismic vibrations, provide ground motion amplification estimates by either comparing to a nearby reference-site where no amplification is expected, i.e., the traditional spectral ratio (SR) method (Borcherdt 1970) or by using the horizontal-to-vertical-spectral-ratio (HVSR) method at a single station (e.g. Nakamura 1989). Instrumental methods do not require prior knowledge of subsurface structure and lithology. However, they lack robustness, as local site effects can considerably change over short distances (Aki 1988).

The SR method, also known as Empirical Transfer Function (ETF), requires simultaneous recordings of earthquake ground motions throughout basin- and reference-sites, a challenging task, especially in urban areas where anthropogenic noise limits the usable magnitudes and even more so in regions with moderate to low seismicity. On the other hand, HVSR methods rely on ambient vibrations (originally referred to as micro-tremors) and do not require recordings at reference-sites (e.g. Ohta et al. 1978; Kagami et al. 1982, 1986; Nakamura 1989). The theoretical basis of the method, however, is still debated as opposite explanations have been proposed and there is no simple correlation between H/V peak values and the actual site amplification factors (Bonnefoy-Claudet et al. 2006). It is generally assumed that HVSR techniques predict the fundamental resonant frequency accurately, however, it is significantly less accurate in predicting amplification factors (Lachetl and Bard 1994; Dravinski et al. 1996; Huang 2002; Rong et al. 2017).

Evidence from ground shaking and site response in the Los Angeles basin, following the 1994 Northridge earthquake (Gao et al. 1996; Hartzell et al. 1997; Graves et al. 1998) and from Kobe, following the 1995 Great Hanshin earthquake (Kawase 1996), showed the importance of understanding the deep basin structure and its effect on ground motions. Specifically, the focusing of seismic energy by geological structures and the interference of surface and body waves at the edge of the basin can result in significant variations in site response over short baselines: up to a factor of 2 over 200 m (e.g. Hartzell et al. 1997). These structure-related aspects of wave propagation are of significant interest in the quantitative evaluation of seismic hazard (e.g., Hatayama et al. 1995; Field 1996; Graves et al. 1998; Joyner 2000; Rovelli et al. 2001; Spudich and Olsen 2001; Adams et al. 2003; Cornou et al. 2003; Wang et al. 2006; Frankel et al. 2009; Hartzell et al. 2010).

2 Seismic hazard of the Haifa Bay

The Zevulun Valley (ZV) is a deep and narrow basin underlying the Haifa Bay, a heavily populated and industrialized region, serving as the main petrochemical hub of Israel. It stretches along a 20 km coastline between the Carmel mountain in the south and the historical city of Acre in the north (Fig. 1). Bounded by the Mediterranean Sea in the west

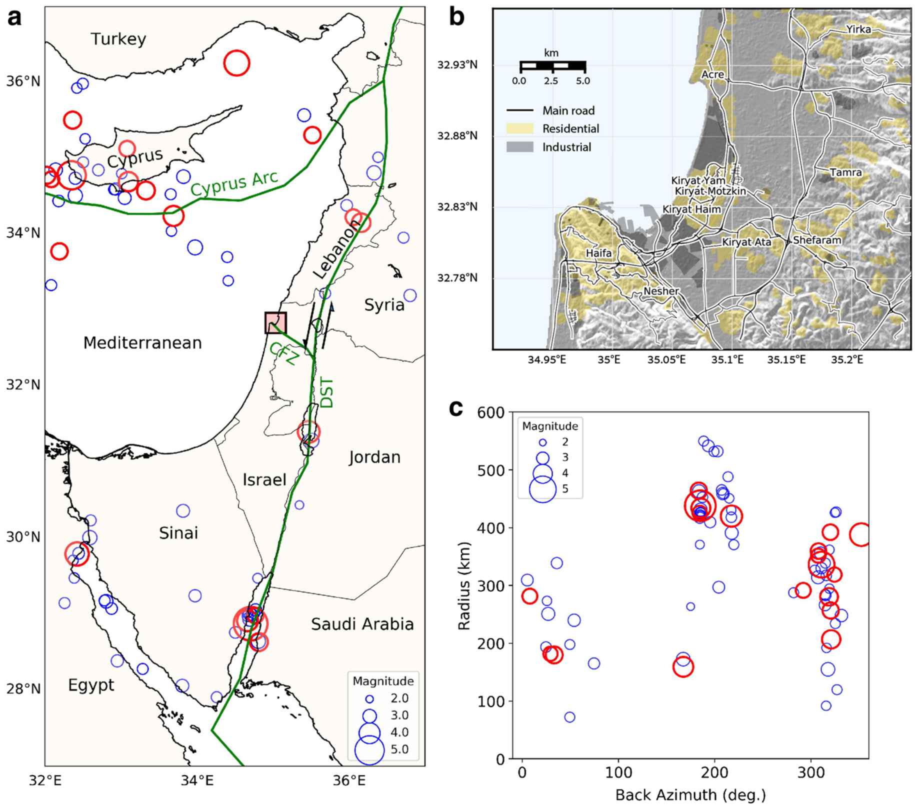

Fig. 1 **a** Location map, regional tectonic borders and seismic events recorded by the Zevulun Valley (ZV) portable array. *DST* Dead Sea Transform, *CFZ* Carmel Fault Zone. The red rectangle is the location of the Haifa Bay; **b** Land use map of the Haifa Bay area; and **c** radius versus back-azimuth of the ZV seismic catalog. Events marked red are 3 < M < 5.5 analyzed in this paper

and the Galilee mountains foothills in the east, it is 9 km wide at its widest point. At the deepest point of the basin the hard carbonate rocks of the Judea Group, considered here as "basement", are more than 1500 m deep. The ZV is in close proximity to active tectonic borders and potentially active faults. Within the basin, several reflectors of high impedance ratios are expected to amplify seismic ground motions.

Tectonic plate boundaries known as contributing factors to seismic hazard in the ZV are: the Dead Sea Transform (DST), less than 50 km away to the east and the Cyprus Arc, approximately 180 km to the north-west (Fig. 1a). The DST is a left-lateral strike slip fault with low strain rate (<4 mm/year), yielding low seismicity rate, with centennial return periods. Detailed pre-instrumental records of the Levant (Eastern Mediterranean) region dates back as far as 1200 BC (Agnon 2014) and includes numerous destructive earthquakes (e.g., the 749 CE, 1202 CE and 1837 CE events, among many others). The 1927 Jericho event with estimated local magnitude of M_L 6.2 was the last strong earthquake on the DST. It resulted in vast devastation and hundreds of casualties out of a total population of about 700,000 (British Palestine). This event predated the accelerated urban and industrial growth of the region in general, and the Haifa Bay area in particular. The subduction zone of the Cyprus Arc is capable of generating earthquakes with magnitudes larger than 6, with return periods of 50 years and larger than 7 with return periods of 500 years (Shapira and Hofstetter 2002).

In August 1984, a magnitude 5.3 earthquake occurred in the Jezreel Valley, about 10 km east of the Zevulun Valley. However, its relation to the Carmel-Gilboa fault system, which bounds the ZV in the south, is unclear. For seismic hazard analysis, it has been suggested to treat the Carmel fault and its southeast continuation (Gilboa fault) as one seismogenic zone, the Carmel Fault Zone (CFZ) capable of generating earthquakes with magnitudes up to M 6.5 (Shamir et al. 2001).

2.1 Ground motion amplification in Haifa Bay

With active tectonic faults at close range and a mixture of large population and vulnerable facilities, the seismic risk in the ZV is elevated. Israel building code SI413, Design Provisions for Earthquake Resistance of Structures, (Israel Standards Institution 2013) addresses ground motion amplification via two basic inputs:

1. Vs30 based (NEHRP) soil classification scheme (Building Seismic Safety Council 2001) for calculation of response spectra amplifications.
2. A map of regions of potential high ground motion amplification. A qualitative product, outlining such regions based on geological knowledge without quantitative dimensions.

Ground motion amplification factors in the ZV were previously estimated using the HVSR technique by the Geophysical Institute of Israel (GII) in a coordinated effort led by Zaslavsky (2006). Gvirtzman and Louie (2010) conducted a 2-D numerical study of ground motions atop of the ZV, which suggested that the deeper parts of the valley (Qishon and Hilazon grabens, described in detail in Sect. 2) are likely to exhibit a basin-wide ground motion amplification by a factor of two with localized factors up to five at certain locations.

In this paper, we introduce a dataset collected during a 16 months' campaign of seismic monitoring with a transportable network consisting of six stations deployed in the ZV. This dataset contains the first simultaneous earthquake ground motion recordings at basin- and reference-sites in Israel. We focus on a subset of small and moderate earthquakes, $3 < Mw < 5.5$, at local and regional distances (Table 1; Fig. 1c), with the best signal-to-noise ratio (SNR), set to a minimum threshold value of 4. We begin with a structural description of the ZV geology, proceed with estimation of measured and modeled ground motion amplification factors, and provide an interpretation of the recordings with regard to the deep geological structure of the basin.

3 Geological structure of the Zevulun Valley

The structural description of the ZV is based on a compilation of previous studies by Sagy and Gvirtzman (2009), who have compiled geological data from 134 water and oil wells and 35 seismic surveys with a total length of more than 300 km. Most of the old seismic surveys, collected in the 1970s, 1980s and 1990s, were reprocessed in 2007 and 2008 using modern processing tools.

The deep structure of the ZV is best visualized by the structural map of top Judea Gr. surface (Fig. 2) which is a significant regional reflector considered here as "basement".

Table 1 List of events used to compute spectral ratios

Date	M_W	Depth (km)	R (km)	Back Azimuth (deg.)	Location	PGA (cm/s^2)
2014.09.01	4.1	10	180	033	Yamune[2]	0.65
2014.09.29	3.7	27	248	331	East Med[3].	0.11
2014.10.25	3.1	3	240	054	Palmira	0.10
2014.11.11	3.4	25	291	291	East Med.	0.40
2015.04.15	4.9	18	336	310	Cyprus Arc	0.70
2015.05.07	3.1	3	251	027	Yamune	0.04
2015.06.17	5.5[1]	10	437	185	Aragonese[4]	1.1
2015.07.08	4.3	5	434	185	Aragonese	0.05
2015.07.17	3.2	32	155	217	East Med.	0.06
2015.07.21	3.8	15	280	319	Cyprus Arc	0.69
2015.07.29	4.1[1]	10	388	352	East Med.	0.37
2015.07.30	4.3[1]	15	159	167	Dead Sea	0.28
2015.07.30	3.9	3.1	207	321	East Med.	0.54
2015.12.11	3.3	20	318	324	Cyprus Arc	0.01
2015.12.20	3.6	15	257	320	East Med.	0.01

1. Felt; 2. Yamune Fault (Lebanon); 3. Eastern Mediterranean; 4. Aragonese Deep—Gulf of Aqaba

This surface reveals a steep, faulted relief buried under a sedimentary fill that forms the present flat topography (near MSL) of the valley. The ZV is a graben-horst-graben structure forming two sub-basins separated by a flat rise. Bounded by East–West striking normal faults (Fig. 2b), the southern graben is the Qishon basin (QG) and the northern graben is the Hilazon basin (HG). Separating them is the Afek Horst (AH). At its southern end, the valley is bounded by the seismically active Carmel fault zone.

Sagy and Gvirtzman (2009) and Gvirtzman et al. (2011) defined six structural reflectors for the ZV (Fig. 2): (1) base of the Kurkar Gr. (Plio-Quaternary)—bK, (2) base of the Pliocene Yafo Fm. (laterally coinciding with the top of the Middle Miocene Ziqlag Fm., top of the Late Miocene Pattish Fm. or top of the Messinian Mavqiim Fm.)—bY, (3) top Bet Guvrin Fm. (Oligocene–Miocene)—tBG, (4) base of the Saqiye Gr. (Late Eocene to Pliocene)—bSq, (5) top Mt Scopus Gr. (Late Cretaceous)—tMS, and (6) top Judea Gr. (Albian-Turonian)—tJ.

Two cross-sections, longitudinal (AA') and transverse (BB'), through the ZV are presented in Fig. 2b, c respectively, illustrating that syn-tectonic units (the Bet Guvrin, Yafo and Patish Fm. of the Saqiye Gr.) thicken in the grabens and thins towards the Afek Horst. The Kurkar Gr. finally covers the entire ZV forming flat topography and leaving no expression for the horst-and-graben structure.

Shear wave velocities of the regional structural units (Judea Gr. Avedat Gr. and Mt. Scopus Gr.) were retrieved from a regional velocity model. Shear wave velocities of the syn-tectonic units (mainly in the Qishon graben) were estimated using empirical density-velocity relations (Brocher 2005) and available borehole density measurements. Where available, velocity values based in inversions of ambient vibrations by Zaslavsky et al. (2008) were used as well. The Kurkar Gr. (Vs = 350 m/s) contains clayey and sandy soils, sand dunes, consolidated sandstones, conglomerates and unconsolidated sands. The underlying Yafo Fm. (Vs = 600 m/s) is composed of marls of shales. The Ziqlag/Patish formations (Vs = 1500 m/s) are composed of

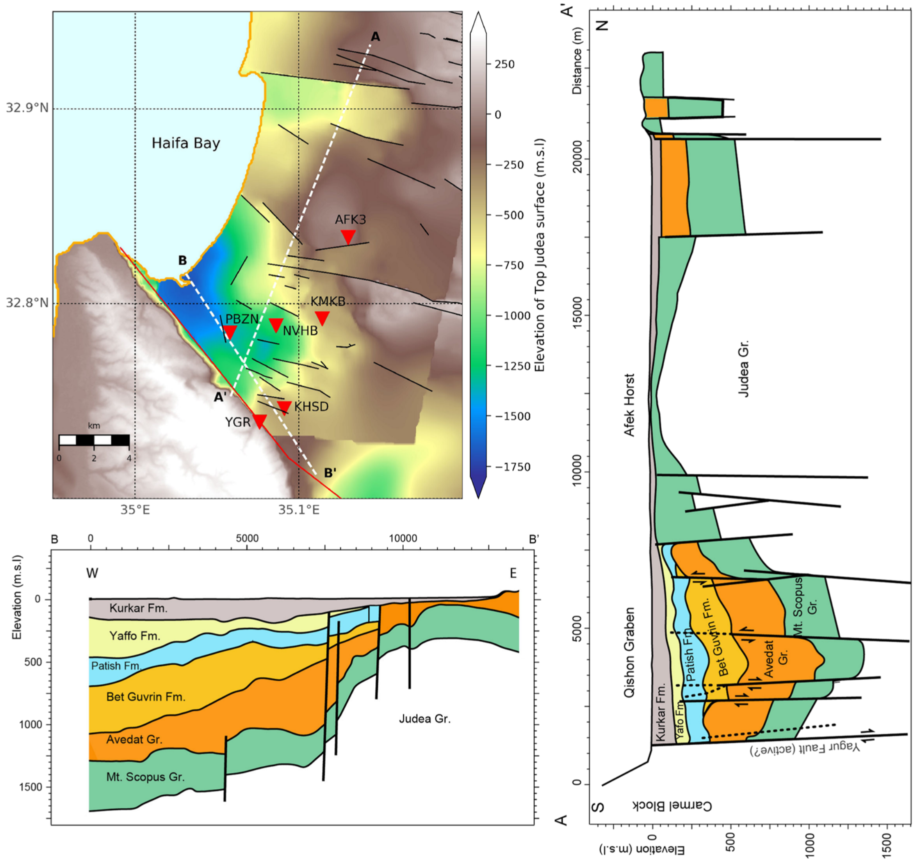

Fig. 2 The geological structure of the Zevulun Valley: **a** depth to Top of Judea structural surface with transportable array stations location (triangles). *QG* Qishon Graben, *AH* Afek Horst, *HG* Hilazon Graben, *m.s.l.* mean sea level. **b** Geological cross-section AA′ (N–S direction). **c** geological cross-section BB′ (E–W direction)

hard limestone. The Mavqiim Fm. (Vs = 1500 m/s) is composed of gypsum. The Bet Guvrin formation (Vs = 800 m/s) is composed of marl. The Avedat Gr. (Vs = 1000 m/s) is composed of chalk and limestone. The Mount Scopus Gr. (Vs = 900 m/s) is composed of soft carbonates. Finally, at the bottom, the Judea Gr. (Vs-2000 m/s) is composed of very hard limestone and dolomite with an impedance ratio of at least 2 with overlying formations.

Noteworthy, a complete stratigraphic section is only present in the QG graben while a partial section is preserved in the nearby the AH. The depth of the Judea Gr. is found at about 1500 m under the QG, and about 400 m under the HG, and almost reaches the surface at the AH (Fig. 2).

4 Instrument deployment

To study the earthquake-induced ground motions in the ZV the Geological Survey of Israel (GSI) deployed a transportable seismic network designed for shallow, quick installation and removal. Six stations were deployed for a period of 16 months (August 2014–December 2015) and maintained by the Geophysical Institute of Israel (GII). The deployed sites were chosen to sample different structural settings of the QG (Fig. 2) while considering practical limitations such as security of equipment and power supply, which contribute to anthropogenic noise. The seismometers were glued to a rock outcrop (YGR1 and KMKB), a concrete foundation (AFK3 and PBZN) or to fresh cement casting in a ~ 0.5 m deep pit (KHSD), and covered with a thermally insulating housing. Locations and technical aspects of installation are given in Table 2. The shear wave velocity profile under each station (Fig. 3) was retrieved from the structural maps of major reflectors described by Sagy and Gvirtzman (2009), see description above.

Station YGR was installed on a hard rock outcrop (Judea Gr.) immediately south of the Carmel escarpment, attached to the Carmel block (Fig. 2). Surface shear wave velocity of the Judea Gr. was measured in the laboratory to be 1800 m/s (Chetrit 2004). This station is the reference-site for other stations located on soft rocks within the basin. Probabilistic Power Spectral Density (PPSD) analysis of background noise (McNamara and Buland 2004) of YGR1 station showed a quiet and stable station: − 150 to − 130 dB from 10 s to 50 Hz. The HVSR (bandpass filtered 0.1 to 10 Hz) of this station (Fig. 4) shows amplification factor of ~ 2 from 1 to 2 Hz which may express near surface weathering and jointing (Steidl et al. 1996).

Station KHSD, 1.5 km north-east of YGR1, was located on the south-eastern edge of the basin on top of the Kurkar Gr. sediments (Vs = 350 m/s) with bK reflector at a depth of 24 m. Two stations were deployed within the deep part of the QG: PBZN and NVHB both located 5.4 km away from the YGR1 reference station. Station PBZN was located over the deepest part of QG, with tJ reflector at a depth of 1400 m. The bY reflector, separating hard limestones (Vs = 1500 m/s) and shales (Vs = 600 m/s) is found at depth of 225 m. PBZN station was located near a major industrial facility with high background noise (higher than -100 dB) centered at a frequency 3 Hz. This unwanted effect was mitigated by applying a bandstop filter at 3 Hz (see Data Processing section). Under NVHB station, the tJ reflector is located at a depth of 1200 m and the bY reflector is at depth of 141 m. Station NVHB was located within a school compound in a dry drainage vault. This station exhibited

Table 2 Zevulun Valley transportable network location, installation type and geological setting

Station	Lon.	Lat.	Installation Type	Geological setting	Bandpass Filtering Range
YGR1	35.075	32.74	Rock	Reference	0.1–10 Hz
PBZN	35.058	32.785	Concrete foundation. Near industrial facility	QG deep.	0.1–10 Hz and Bandstop 3 Hz
NVHB	35.086	32.788	Vault. School compound.	QG deep.	0.25–10 Hz
KMKB	35.114	32.792	Rock	QG shallow	0.1–10 Hz
KHSD	35.091	32.746	Soil (0.5 m)	QG shallow	0.1–10 Hz
AFK3	35.130	32.834	Concrete foundation	Afek Horst	0.1–10 Hz

QG Qishon Graben

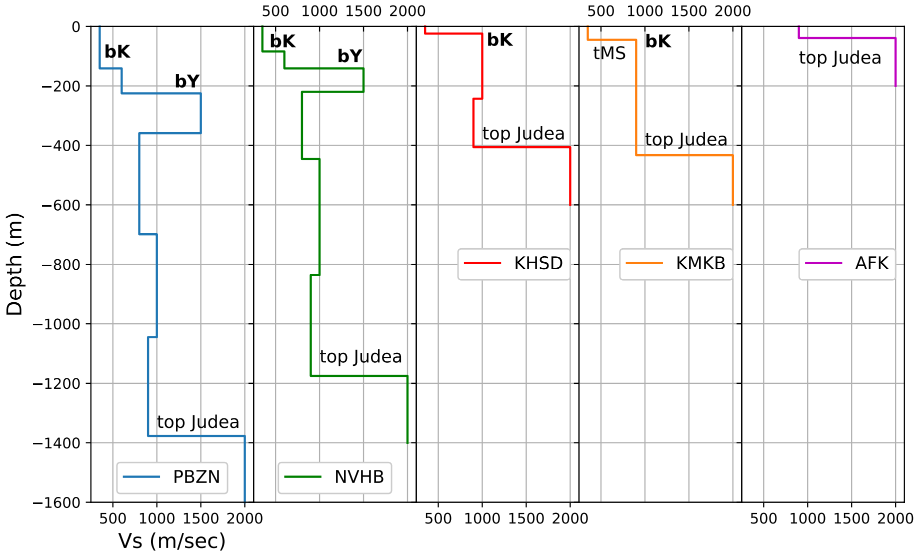

Fig. 3 Vertical velocity profiles of the Zevulun Valley transportable network stations. *bK* base Kurkar Gr. reflector, *bY* base Yaffo Fm. reflector

Fig. 4 Horizontal to vertical spectral ratio of station YGR, located on rock immediately south of the Carmel Fault escarpment

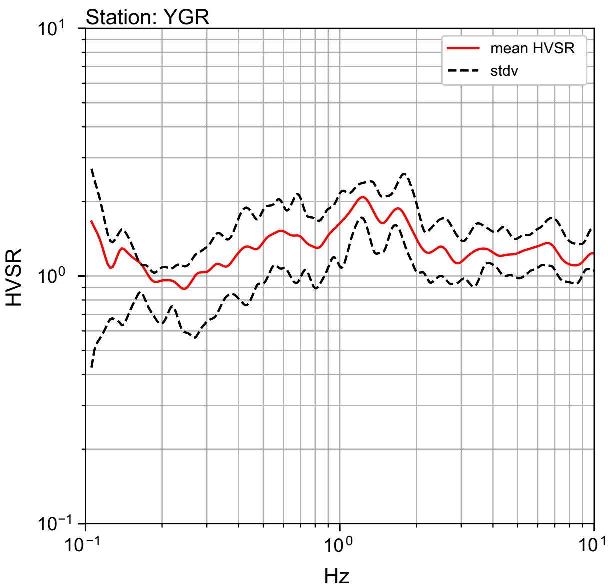

tangible background noise at low frequencies (<0.25 Hz) most probably due to a wind-induced loading of tall trees near the vault.

Station KMKB is similar in nature to station KHSD, deployed over the shallow (eastern) part of QG (Fig. 2). Station AFK was deployed on a rock site at the eastern part of the Afek Horst, but differing from the reference station (YGR1) located on the Judea Gr. (Vs = 2000 m/s), AFK was built on the Mount Scopus Gr. (Vs = 900 m/s).

5 Data processing

Raw data recorded during earthquakes was extracted from continuous recordings using the time stamp of the Israeli Seismic Catalog (published by the GII). These waveforms were demeaned, tapered with a 5% cosine taper, band-pass filtered between 0.1 and 10 Hz and corrected for instrument response. In the case of the PBZN station (near the Haifa Bay Refineries) it was necessary to also apply a bandstop (notch) filter in order to remove anthropogenic noise centered at 3 Hz. Station NVHB was bandpass filtered from 0.25 to 10 Hz in order to avoid natural background noise at low frequencies.

Wave spectra were computed from the processed waveforms using 120 s time windows covering the p and s waves windows of the record and smoothed using logarithmic smoothing function (Konno and Ohmachi 1998). For each station in the basin, spectral amplification ratios were computed relative to YGR1 and averaged over all available events. SNR was computed for each station-event pair using the spectral approach (Bormann 1998) for 0.1–1 Hz and 1–5 Hz windows. The higher frequency window was found to be significantly noisier due to the strong anthropogenic noise in the region. However, SNR was typically above 4 and even at noisy stations like PBZN SNR at the 0.1–1 Hz band was above 10.

6 Ground motions and spectral amplifications

The strongest earthquake in the ZV catalog is the Mw 5.5 Nuweiba earthquake (Table 1), with an epicentral distance of 437 km and back azimuth of 184°. Relative to the aperture size of the network (~10 km), the epicentral distance is sufficient to assume that any variation in the recorded ground motions is a result of the basin response. The three components of the ground motion (radial, transverse and vertical) for each station in the ZV array are presented in Fig. 5. The strong amplification of ground motions over the deep parts of the ZV is evident. Stations PBZN and NVHB exhibit higher amplitudes (by order of magnitude relative to the reference station YGR) and prolonged duration of shaking whereas stations KHSD, KMKB located over the shallow parts of the ZV show lower amplification. Station AFK3, situated on the horst separating the two grabens of the ZV shows similar ground motions to the reference station of YGR.

In order to characterize the amplification factor as a function of frequency, spectral amplification of the radial and transverse components for 15 earthquakes, $3 < M < 5.5$ (Table 1), are averaged for stations PBZN, NVHB, KMKB and KHSD (Fig. 6). The arithmetic mean of spectral ratios is plotted using a dashed line with gray filling denoting one standard deviation (stdv). For comparison, one-dimensional (1D) linear elastic transfer function corresponding to the velocity profile at each station is also plotted (solid line). This 1D transfer function was computed using the Strata software (Kottke and Rathje 2008). The linear elastic assumption was found to be appropriate for this case as the maximum shear strain, 5×10^{-5} at the PBZN station, is near the non-linear strain threshold of 10^{-4} (Bereznev and Wen 1996; Kaklamanos et al. 2015) and in most of the events reported here is about 10^{-6}.

Measured amplifications at station PBZN, over the deepest part of the basin (Fig. 6), exhibit comparable spectral features to the 1D transfer function. The two main reflectors, tJ and bY (depth of 1377 and 225 m, respectively), account for strong amplification at 0.16 and 0.5 Hz, respectively as these are the expected fundamental frequencies. However,

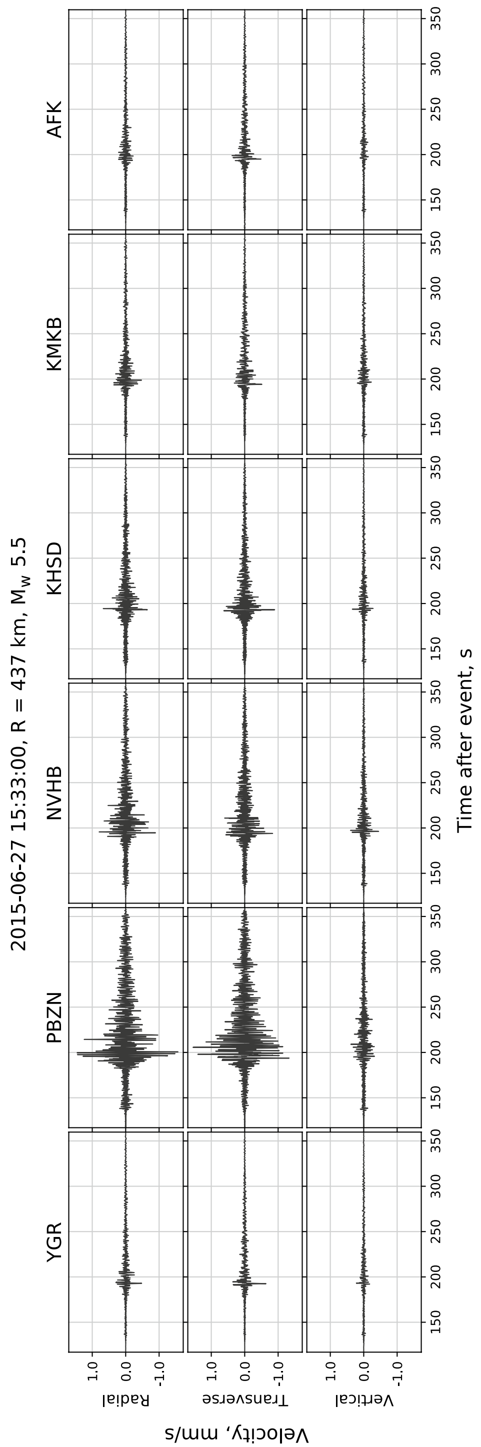

Fig. 5 Recorded ground motions for the Nuweiba M_w 5.5 earthquake. R, T and Z are radial, transverse and vertical components, respectively

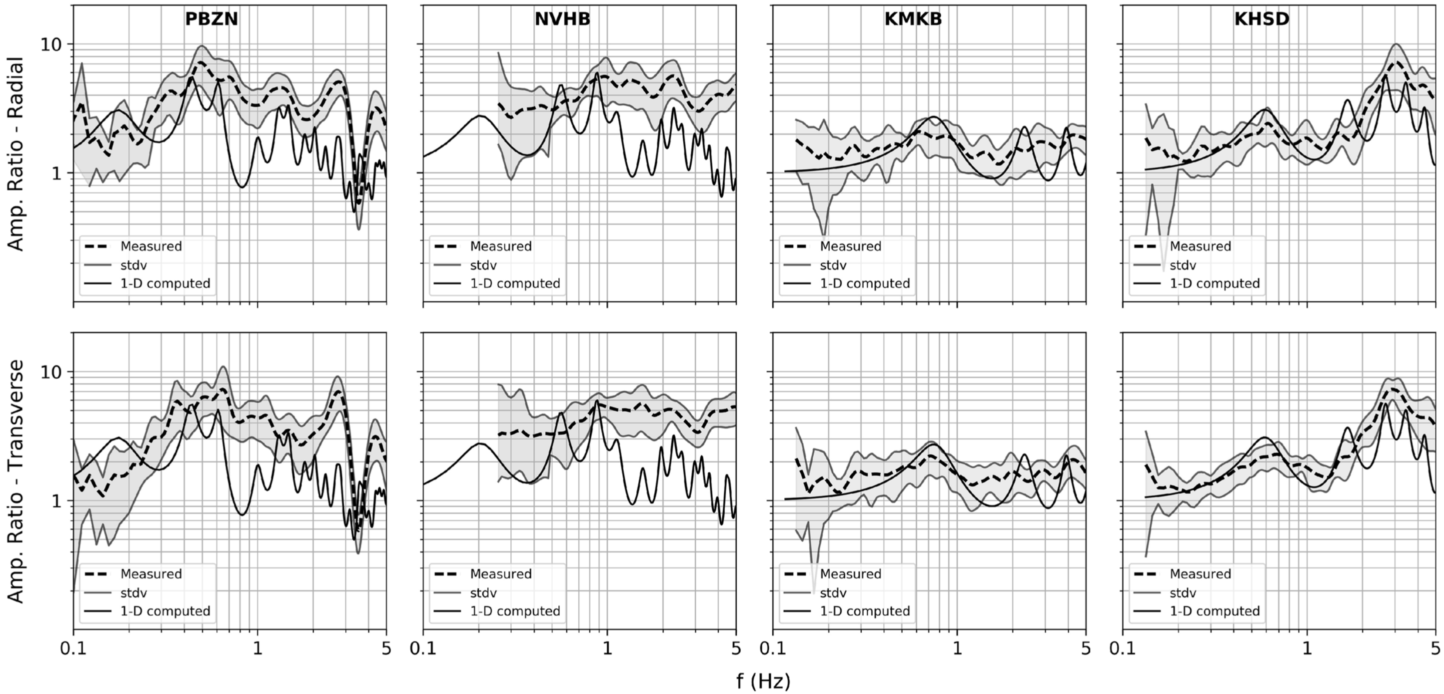

Fig. 6 Spectral ground motion amplifications for the Radial component (upper panel) and Transverse component (lower panel) of the Zevulun Valley Network computed relative to YGR reference station, for earthquakes listed in Table 1. The dashed line is average instrumental value, shaded area is one standard deviation from the average and the continuous line is 1-D linear elastic transfer function

spectral amplification ratios are higher than predicted by the 1D approach. Specifically, for the 0.5 Hz peak, where the measured amplification ratio is 7 (and up 10 with 1 stdv) compared to 5 of the 1D result. In the 1–3 Hz frequency band, the measured amplification ratio is 4–5, whereas the 1D amplification is lower, 3 at 1.5 Hz. The biggest discrepancy between the measured and modeled amplification is obtained for a frequency of ~2.5 Hz where the 1D model doesn't predict the observed amplification of factor 6.

Station NVHB exhibits amplification by a factor of 3 for frequencies lower than 1 Hz and with a rather large standard deviation towards the lower frequencies. For the frequency band 1 to 2 Hz the amplification factor rises to a value of 5, falling again to a factor of 3 for frequencies higher than 2 Hz. Similar to station PBZN the 1-D model doesn't predict the high amplification observed for frequencies larger than 1 Hz, but reaches a general agreement with observations for frequencies lower than 1 Hz.

Amplification ratios at stations KMKB and KHSD (Fig. 6), situated over the shallow part of the basin, are in good agreement with 1D predicted amplifications both in terms of frequency and magnitude. Specifically, at 0.6 Hz (tJ reflector at depth of 377 m) and also at 3 Hz (bK reflector at 24 m depth) at KHSD. Amplifications at station AFK3 (located on rock) are not presented here as no significant amplification was observed or computed for this surface rock station.

7 Discussion and conclusions

The new earthquake recordings atop the structurally complex Zevulun Valley (ZV) provide first of their kind measurements allowing seismic hazard assessment for this vulnerable region. The results presented here significantly differ from previous estimates either based on HVSR measurements of ambient noise (Zaslavsky et al. 2008) or on 2D numeric modeling (Gvirtzman and Louie 2010). Zaslavsky et al. (2008) published maps of fundamental and second resonant peaks with their associated amplification ratios for the Qishon Graben. Gvirtzman and Louie (2010) performed 2-D numerical analysis of wave propagation (frequency range of 0.2–6 Hz) for the cross-section presented in Fig. 2c using the velocity model described above. Comparison between the new results reported here and previously published results for the locations of our stations are presented in Table 3.

The two deep basin stations, PBZN and NVHB, with their two typical resonant peaks (below and above 1 Hz) exhibit the strongest discrepancy between new and previous

Table 3 Comparison of dominant frequencies and amplification factors from three different methods: HVSR (Zaslavsky et al. 2008), 2-D finite difference wave propagation modeling (Gvirtzman and Louie 2010) and measured spectral ratios (SR, arithmetic mean of amplification peaks of horizontal components)

Station	HVSR				2-D model				SR			
	f_0 (Hz)	AF_0	f_1 (Hz)	AF_1	f_0 (Hz)	AF_0	f_1 (Hz)	AF_1	f_0 (Hz)	AF_0	f_1 (Hz)	AF_1
PBZN	0.6	4	1	2	0.4	5	MP	2	0.5	7	2.5	7
NVHB	0.5	2	1.5	4	0.5	5	MP	2	0.4	4	2.5	6
KMKB	0.8	2	N/A	N/A	N/A	N/A	N/A	N/A	0.8	3	> 1	< 2
KHSD	0.8	2.5	4	4	0.7	4	2.5	5	0.6	3	3	8

f_0 and f_1 are first and second resonant frequencies and AF is Amplification Factor. Locations of stations are projected to the 2-D model locations. MP stands for multiple peaks at $f > 1$ Hz results. For instance, in the PBZN station, the HVSR method yields amplification factors of 4 and 2 for lower and higher frequency peaks, respectively (Zaslavzky et al. 2008), while the SR methods in this study yields factors of 7 for both peaks (Table 3). Such a discrepancy between the HVSR and SR the methods are well documented in the scientific literature. Recently, Rong et al. (2017) suggested that the underlying assumption of the Nakamura HVSR method, that the vertical response at a site is unamplified is not accurate.

Comparison of the SR method (this study) with 2-D modeling results (Gvirtzman and Louie 2010) for deep basin stations shows good agreement for the lower frequency peak (AF ~ 2.5), but not for the high frequency peak where, again, the SR method yields significantly higher amplification factor of ~ 8 (Table 3). One should recall that the high amplification factors obtained for the high frequencies may even be underestimated, because the YGR reference station exhibits minor amplification at 1 to 2 Hz frequency band (Fig. 4), thus lowering the amplification ratio of the basin stations in this particular band.

It is worth mentioning that spectral amplification ratios larger than 7, although high, are not unprecedented. Similar factors were observed in Mexico City following the 1985 M_w 8.0 earthquake (Romo and Seed 1986; Seed et al. 1987) and later confirmed during the 2017 earthquakes (Sahakian et al. 2018). In Takai et al. (2016) spectral amplification ratios larger than 10 are discussed for the Kathmandu valley during the 2015 M_w 7.8 Gorkha earthquake. The results presented here should be used within the limitations of the dataset, mainly low strain ground motions in the linear range, and should be regarded as general trends. Extrapolation to strong motion amplifications should address soil non-linearity and associated energy dissipation which may result in decrease of the fundamental frequency and amplification factor.

The epicentral distances to the ZV network stations and earthquake magnitudes recorded during this campaign are such that strain levels at the measuring sites were low, $< 10^{-5}$. Therefore, we did not account for soil non-linearity in our analysis. Future studies aimed to quantify the seismic hazard of the ZV should address the effects of soil non-linearity which include resonant peak shift, toward lower frequencies, and lower amplification ratios.

The above results and insights are essential for seismic hazard mitigation in the Haifa Bay metropolitan area, in which residential neighborhoods and sensitive petrochemical and other industrial facilities are intertwined. The deep structure of the Zevulun basin is clearly reflected in the recorded ground motions.

For the first time in Israel earthquake ground motions were recorded simultaneously at basin- and reference-sites. Ground motion amplification factors reported here are higher than those previously estimated using HVSR of micro-tremors (Zaslavsky et al. 2008) or 2D modeling (Gvirtzman and Louie 2010). In particular, at deep basin sites, we observe strong low frequency (~ 0.5 Hz) amplification factors reaching amplitudes of 10 for single events and 7 on average. These amplifications are pertinent to low-period (high-rise) residential buildings and tall industrial facilities such as oil refineries and distillation towers among others.

8 Data and resources

We have used the Israel Seismic Catalog maintain by the Geophysical Institute of Israel (GII), available at http://seis.gii.co.il/heb/earthquake/searchEQS.php. Seismograms used in this study were collected using a temporary deployment of the GSI transportable array maintained by GII. The data is available upon request from the GII. Data was processed using the ObsPy (Beyreuther et al. 2010) package ver. 1.0.3.

Acknowledgements The portable seismic network used to collect the data for this study was purchased by the Geological Survey of Israel with funds provided by the Ministry of Energy and Water.

References

Adams BM, Osborne NM, Taber JJ (2003) The basin-edge effect from weak ground motions across the fault-bounded edge of the lower Hutt Valley. N Z Bull Seismol Soc Am 93:2703–2716. https://doi.org/10.1785/0120010277

Agnon A (2014) Pre-instrumental earthquakes along the Dead Sea Rift. In: Garfunkel Z, Ben-Avraham Z, Kagan E (eds) Dead sea transform fault system: reviews. Springer, Dordrecht, pp 207–262

Aki K (1988) Local site effects on strong ground motion. In: Paper presented at the Earthquake engineering and soil dynamics II—recent advances in ground-motion evaluation

Aki K, Larner KL (1970) Surface motion of a layered medium having an irregular interface due to incident plane SH waves. J Geophys Res 75:933–954. https://doi.org/10.1029/JB075i005p00933

Alex CM, Olsen KB (1998) Lens effect in Santa Monica? Geophys Res Lett 25:3441–3444. https://doi.org/10.1029/98gl52668

Bereznev IA, Wen K (1996) Nonlinear soil response—a reality? Bull Seismol Soc Am 86:1964–1978

Beyreuther M, Barsch R, Krischer L, Megies T, Behr Y, Wassermann J (2010) ObsPy: a python toolbox for seismology. Seismol Res Lett 81:530–533. https://doi.org/10.1785/gssrl.81.3.530

Bonnefoy-Claudet S, Cotton F, Bard P-Y (2006) The nature of noise wavefield and its applications for site effects studies: a literature review. Earth Sci Rev 79:205–227. https://doi.org/10.1016/j.earscirev.2006.07.004

Borcherdt RD (1970) Effects of local geology on ground motion near San Francisco Bay. Bull Seismol Soc Am 60:29–61

Bormann P (1998) Conversion and comparability of data presentations on seismic background noise. J Seismol 2:37–45. https://doi.org/10.1023/a:1009780205669

Brocher TM (2005) Empirical relations between elastic wavespeeds and density in the earth's crust. Bull Seismol Soc Am 95:2081–2092. https://doi.org/10.1785/0120050077

Building Seismic Safety Council (2001) NEHRP recommended provisions for seismic regulations for new buildings and other structures, Part 1: provisions (FEMA 368)

Chetrit M (2004) Subsurface structure of the NW coast of the Dead Sea: a geophysical study. M.Sc. Thesis (in Hebrew). Ben Gurion University of the Negev

Cornou C, Bard P-Y, Dietrich M (2003) Contribution of dense array analysis to the identification and quantification of basin-edge-induced waves. Part I: methodology. Bull Seismol Soc Am 93:2604–2623. https://doi.org/10.1785/0120020139

Dravinski M, Ding G, Wen K-L (1996) Analysis of spectral ratios for estimating ground motion in deep basins. Bull Seismol Soc Am 86:646–654

Field EH (1996) Spectral amplification in a sediment-filled Valley exhibiting clear basin-edge-induced waves. Bull Seismol Soc Am 86:991–1005

Frankel A, Stephenson W, Carver D (2009) Sedimentary basin effects in Seattle, Washington: ground-motion observations and 3D simulations. Bull Seismol Soc Am 99:1579–1611. https://doi.org/10.1785/0120080203

Gao S, Liu H, Davis PM, Knopoff L (1996) Localized amplification of seismic waves and correlation with damage due to the Northridge earthquake: evidence for focusing in Santa Monica. Bull Seismol Soc Am 86:S209–S230

Graves RW, Pitarka A, Somerville PG (1998) Ground-motion amplification in the Santa Monica area: effects of shallow basin-edge structure. Bull Seismol Soc Am 88:1224–1242

Gutenberg B (1957) Effects of ground on earthquake motion. Bull Seismol Soc Am 47:221–250

Gvirtzman Z, Louie JN (2010) 2D analysis of earthquake ground motion in Haifa Bay, Israel. Bull Seismol Soc Am 100:733–750. https://doi.org/10.1785/0120090019

Gvirtzman Z, Makowski I, Sagee Y (2011) Re-processing and geological re-interpretation of old seismic lines of Haifa bay. Geological Survey of Israel. GSI/27/2011

Hartzell S, Cranswick E, Frankel A, Carver D, Meremonte M (1997) Variability of site response in the Los Angeles urban area. Bull Seismol Soc Am 87:1377–1400

Hartzell S, Ramirez-Guzman L, Carver D, Liu P (2010) Short baseline variations in site response and wave-propagation effects and their structural causes: four examples in and around the Santa Clara Valley, California. Bull Seismol Soc Am 100:2264–2286. https://doi.org/10.1785/0120090278
Hatayama K, Matsunami K, Tomotaka I, Kojiro I (1995) Basin-induced love waves in the eastern part of the Osaka Basin. J Phys Earth 43:131–155. https://doi.org/10.4294/jpe1952.43.131
Huang H-C (2002) Characteristics of earthquake ground motions and the H/V of microtremors in the south-western part of Taiwan. Earthq Eng Struct Dyn 31:1815–1829. https://doi.org/10.1002/eqe.191
Hudson DE (1972) Local distribution of strong earthquake ground motions. Bull Seismol Soc Am 62:1765–1786
Israel Standards Institution (2013) Standard SI 413. Design Provisions for Earthquake Resistance of Structures. Amendment No. 5
Joyner WB (2000) Strong motion from surface waves in deep sedimentary basins. Bull Seismol Soc Am 90:S95–S112. https://doi.org/10.1785/0120000505
Kagami H, Duke CM, Liang GC, Ohta Y (1982) Observation of 1- to 5-second microtremors and their application to earthquake engineering. Part II. Evaluation of site effect upon seismic wave amplification due to extremely deep soil deposits. Bull Seismol Soc Am 72:987–998
Kagami H, Okada S, Shiono K, Oner M, Dravinski M, Mal AK (1986) Observation of 1- to 5-second microtremors and their application to earthquake engineering. Part III. A two-dimensional study of site effects in the San Fernando Valley. Bull Seismol Soc Am 76:1801–1812
Kaklamanos J, Baise LG, Thompson EM, Dorfmann L (2015) Comparison of 1D linear, equivalent-linear, and nonlinear site response models at six KiK-net validation sites. Soil Dyn Earthq Eng 69:207–219. https://doi.org/10.1016/j.soildyn.2014.10.016
Kawase H (1996) Cause of the damage belt in Kobe: "The Basin-edge Effect", constructive interference of the direct S Wave with the basin-induced diffracted/Rayleigh Waves. Seismol Res Lett 67:5–25
Konno K, Ohmachi T (1998) Ground-motion characteristics estimated from spectral ratio between horizontal and vertical components of microtremor. Bull Seismol Soc Am 88:228–241
Kottke A, Rathje EM (2008) Semi-automated procedure for selecting and scaling recorded earthquake motions for dynamic analysis. Earthq Spectra 24:911–932. https://doi.org/10.1193/1.2985772
Lachetl C, Bard P (1994) Numerical and theoretical investigations on the possibilities and limitations of Nakamura's technique. J Phys Earth 42:377–397. https://doi.org/10.4294/jpe1952.42.377
McNamara DE, Buland RP (2004) Ambient noise levels in the continental United States. Bull Seismol Soc Am 94:1517–1527. https://doi.org/10.1785/012003001
Nakamura Y (1989) A method for dynamic characteristics estimation of subsurface using microtremor on the ground surface. Q Rep Railw Tech Res 30(1):25–33
Ohta Y, Kagami H, Goto N, Kudo K (1978) Observation of 1- to 5-second microtremors and their application to earthquake engineering. Part I: comparison with long-period accelerations at the Tokachi-oki earthquake of 1968. Bull Seismol Soc Am 68:767–779
Romo MP, Seed HB (1986) Analytical modeling of dynamic soil response in Mexico earthquake of September 19th 1985. In: Proceedings of International Conference on the 1985 Mexico Earthquake, Mexico City, 19–21 September 1986, pp 148–162
Rong M, Fu L-Y, Wang Z, Li X, Carpenter NS, Woolery EW, Lyu Y (2017) On the amplitude discrepancy of HVSR and site amplification from strong-motion observations. Bull Seismol Soc Am 107:2873–2884. https://doi.org/10.1785/0120170118
Rovelli A, Scognamiglio L, Marra F, Caserta A (2001) Edge-diffracted 1-Sec surface waves observed in a small-size intramountain basin (Colfiorito, Central Italy). Bull Seismol Soc Am 91:1851–1866. https://doi.org/10.1785/0120000301
Sagy Y, Gvirtzman G (2009) Subsurface mapping of the Zevulun Valley (Hebrew). The Geophysical Institute of Israel, Report 648/454/09
Sahakian VJ, Melgar D, Quintanar L, Ramírez-Guzmán L, Pérez-Campos X, Baltay A (2018) Ground Motions from the 7 and 19 September 2017, Tehuantepec and Puebla-Morelos, Mexico, Earthquakes. Bull Seismol Soc Am. https://doi.org/10.1785/0120180108
Seed HB, Romo MP, Sun J, Jaime A, Lysmer J (1987) Relationships between Soil Conditions and Earthquake ground motions in Mexico City in the earthquake of September 19, 1985. UCB/EERC-87/15, University of California, Berkeley, p 125
Shamir G, Bartov Y, Sneh A, Fleischer L, Arad V, Rosensaft M (2001) Preliminary seismic zonation for Israel. GII Rept. No. 550/95/01(1)
Shapira A, Hofstetter A (2002) Seismicity Parameters of Seismogenic Zones. Geophysical Institute of Israel. Report Num. 592/230/02
Spudich P, Olsen KB (2001) Fault zone amplified waves as a possible seismic hazard along the Calaveras Fault in central California. Geophys Res Lett 28:2533–2536. https://doi.org/10.1029/2000gl011902

Steidl JH, Tumarkin AG, Archuleta RJ (1996) What is a reference site? Bull Seismol Soc Am 86:1733–1748
Takai N, Shigefuji M, Rajaure S, Bijukchhen S, Ichiyanagi M, Dhital MR, Sasatani T (2016) Strong ground motion in the Kathmandu Valley during the 2015 Gorkha, Nepal, earthquake Earth. Planets Space 68:10. https://doi.org/10.1186/s40623-016-0383-7
Trifunac MD, Udwadia FE (1974) Variations of strong earthquake ground shaking in the Los Angeles area. Bull Seismol Soc Am 64:1429–1454
Wang G-Q, Tang G-Q, Boore DM, Van Ness Burbach G, Jackson CR, Zhou X-Y, Lin Q-L (2006) Surface waves in the Western Taiwan Coastal Plain from an aftershock of the 1999 Chi-Chi, Taiwan, Earthquake. Bull Seismol Soc Am 96:821–845. https://doi.org/10.1785/0120050088
Zaslavsky Y et al. (2006) Empirical determinations of local site effect using ambient vibration measurements for the earthquake hazard and risk assessment to Qrayot-Haifa Bay areas. Geophysical Institute of Israel. Report Num. 595/064/06
Zaslavsky Y et al. (2008) Empirical determination of site effects for seismic hazard assessment in the Kishon graben area near the Carmel fault. Geophysical Institute of Israel. Report Num. 510/389/08